Polyhedron 64 (2013) 91–98

Contents lists available at SciVerse ScienceDirect

Polyhedron

journal homepage: www.elsevier.com/locate/poly

Rare nuclearities, new structural motifs, and slow magnetization relaxation phenomena in manganese cluster chemistry: A $Mn_{15}Na_2$ cage from the use of triethanolamine/pivalate/azide "blend"

Dimitris I. Alexandropoulos [a], Eleni C. Mazarakioti [b], Simon J. Teat [c], Theocharis C. Stamatatos [a,*]

[a] Department of Chemistry, Brock University, St. Catharines, Ontario, Canada L2S 3A1
[b] Department of Chemistry, University of Patras, Patras 26500, Greece
[c] Advanced Light Source, Lawrence Berkeley National Laboratory, 1 Cyclotron Road, Mail Stop 2-400, Berkeley, CA 94720, USA

ARTICLE INFO

Article history:
Available online 6 March 2013

Dedicated to Drago Professor George Christou on the occasion of his 60th birthday and his contributions to molecular cluster chemistry, molecular magnetism and bioinorganic chemistry.

Keywords:
Azides
Carboxylates
Manganese
Pentadecanuclearity
Triethanolamine
Slow magnetization relaxation

ABSTRACT

The combination of azide, carboxylate (pivalate and *in situ* generated formate) and triethanolamine ligands in higher oxidation state Mn cluster chemistry has afforded a new pentadecanuclear, mixed-valence(II,III) compound with a large *S* and a negative *D* value. The unprecedented $[Mn^{II}_2Mn^{III}_{13}]$ cluster exhibits frequency-dependent out-of-phase (χ''_M) signals, characteristics of the superparamagnetic-like slow relaxation of an SMM.

1. Introduction

It is more than two decades since G. Christou initialized a revolution in polynuclear manganese compounds (clusters) at moderate-to-high oxidation states. Undoubtedly, there is no other more suitable word than the "revolution" one, describing the numerous breakthroughs of G. Christou in Mn coordination chemistry and its applications to the fields of molecular magnetism, bioinorganic chemistry, molecular nanoscience and catalysis. Representative examples include (i) the discovery and development of the single-molecule magnetism (SMM) phenomenon [1], (ii) the synthesis and study of the *Drosophila* of SMMs, a $[Mn_{12}O_{12}(O_2CR)_{16}(L)_4]^{0/n-}$ (R = various; L = terminal solvate molecules; n = 1–3) family of clusters with more than 50 siblings [2], (iii) the observation for a first time of exchange-biased quantum tunneling in SMMs [3], (iv) the employment of various new pyridyl alkoxide-based chelate ligands, and ligand "blends" (i.e. pseudohalides and chelate organic groups) in Mn cluster chemistry [4], (v) the synthesis of the largest in nuclearity 3d-metal SMM, namely a giant $[Mn_{84}]$ torus [5], (vi) the targeted modification and structural perturbation of SMM or non-SMM species to enhance or alter their magnetic properties, respectively, in a deliberate way [6], (vii) the initial observation of magnetization hysteresis and quantum tunneling steps in heterometallic Mn–Ln (Ln = lanthanides) SMMs [7], (viii) the synthesis of molecular models of the oxygen-evolving complex of photosystem II [8], with the recent $[Mn^{IV}_3Ca_2]$ compound being the most accurate synthetic model of the OEC metallocore [9], and finally (ix) the employment of molecular clusters and SMMs in oxidation catalysis [10]. Such pioneer work has been followed and extended further towards the same or different directions by an appreciable number of inspired new scientists with interests in synthetic inorganic chemistry, coordination chemistry, bioinorganic chemistry, and molecular magnetism [11].

SMMs are individual molecules that function as single-domain nanoscale magnetic particles [1]. A SMM derives its properties from a combination of a large ground-state spin (*S*) value and an easy-axis type of magnetoanisotropy (negative zero-field splitting

* Corresponding author. Tel.: +1 905 688 5550x3400; fax: +1 905 682 9020.
E-mail addresses: tstamatatos@brocku.ca, theocharisstamatatos@gmail.com (T.C. Stamatatos).

0277-5387/$ - see front matter © 2013 Elsevier Ltd. All rights reserved.
http://dx.doi.org/10.1016/j.poly.2013.02.055

parameter, D), which results in a significant energy barrier to reversal of the magnetization vector, experimentally observed by the appearance of frequency-dependent out-of-phase (χ''_M) AC signals and magnetization hysteresis. Such species also straddle the classical/quantum interface by displaying not just classical magnetization hysteresis but also quantum tunnelling of magnetization (QTM) [12] and quantum phase interference [13]. Thus, SMMs represent a molecular ('bottom-up') route to nanoscale magnetism [14], with potential technological applications in information storage and spintronics at the molecular level [15a], and use as quantum bits (qubits) in quantum computation [15b].

Although compounds displaying SMM behavior are known for several metals, manganese cluster chemistry has been the most fruitful source to date giving a wide range of Mn_x nuclearities. For these reasons, we are developing new synthetic methods to Mn clusters of various nuclearities and structural types, targeting at the stabilization of as many Mn^{III} ions as possible within the molecular species. This is due to the fact that a large molecular magnetoanisotropy of the easy-axis-type would primarily result from the individual Jahn–Teller distorted Mn^{III} centres [16]. In particular, we have recently initiated a program aiming at the investigation of the coordination affinity of N_3^- ion in higher oxidation state Mn cluster chemistry and in reactions with several families of versatile chelates, such as pyridyl or non-pyridyl alcohols, in the additional presence or absence of ancillary carboxylate groups [17]. From a magnetic viewpoint, the N_3^- ion bridging in the 1,1-fashion (end-on) is one of the strongest ferromagnetic mediators in molecular magnetism for a wide range of M–N–M angles [18], while triethanolamine ($teaH_3$) chelate, for example, exhibits an impressive coordinating versatility with metal centers [19]; thus, their amalgamation provided an attractive route to new high-nuclearity/high-spin Mn clusters and SMMs [20].

In the present work, we report the synthesis, structural and magnetic characterization of a new pentadecanuclear, mixed-valence(II/III) Mn cluster with $RCO_2^-/N_3^-/tea^{3-}$ ligation and a cage-like conformation possessing two additionally coordinated Na^+ atoms. The obtained $[Mn^{II}_2Mn^{III}_{13}Na_2]$ cluster exhibits a large ground-state spin (S) value and shows frequency-dependent out-of-phase signals indicative of the slow magnetization relaxation of an SMM.

2. Experimental

2.1. General and physical measurements

All manipulations were performed under aerobic conditions using materials (reagent grade) and solvents as received. *Caution!* Although no such behavior was observed during the present work, perchlorate and azide salts are potentially explosive; such compounds should be synthesized and used in small quantities, and treated with utmost care at all times.

Infrared spectra were recorded in the solid state (KBr pellets) on a Nicolet Nexus 670 FTIR spectrometer in the 450–4000 cm^{-1} range. Elemental analyses (C, H, and N) were performed on a Perkin–Elmer 2400 Series II Analyzer. Variable-temperature direct current (dc) and alternating current (ac) magnetic susceptibility data were collected on a Quantum Design MPMS-XL SQUID susceptometer equipped with a 7 T magnet and operating in the 1.8–300 K range. Sample was embedded in solid eicosane to prevent torquing. Ac magnetic susceptibility measurements were performed in an oscillating ac field of 3.5 G and a zero dc field; the oscillation frequencies were in the 50–1000 Hz range. Pascal's constants were used to estimate the diamagnetic corrections, which were subtracted from the experimental susceptibilities to give the molar paramagnetic susceptibilities (χ_M).

2.2. Compound preparation

2.2.1. $[Mn_{15}Na_2O_8(OH)_2(OMe)(N_3)_2(O_2CH)(O_2CBu^t)_{11}(tea)_4(MeOH)]$ (**1**)

Solid $Mn(ClO_4)_2{\cdot}6H_2O$ (0.36 g, 1.0 mmol), $NaO_2CBu^t{\cdot}H_2O$ (0.25 g, 2.0 mmol), and NaN_3 (0.13 g, 2.0 mmol) were added to a stirred, colorless solution of $teaH_3$ (0.13 mL, 1.0 mmol) and NEt_3 (0.14 mL, 1.0 mmol) in MeCN/MeOH (15 mL, 2:1 v/v). The resulting red solution was stirred for 10 h, during which time all the solids dissolved and the color of the solution changed to dark brown. The solution was filtered, and the filtrate left undisturbed to concentrate slowly by evaporation. After 3 days, X-ray quality brown needle-like crystals of **1** had appeared and were collected by filtration, washed with cold MeCN (2 × 3 mL), and dried under vacuum. Typical yields were in the 40–45% range. The vacuum-dried solid was analyzed as solvent-free **1**. *Anal.* Calc. for $C_{82}H_{157}Mn_{15}Na_2N_{10}O_{48}$: C, 33.72; H, 5.42; N, 4.79. Found: C, 33.51; H, 5.28; N, 4.96%. IR data (KBr pellet, cm^{-1}): ν = 3450mb, 2958m, 2870w, 2101s, 1600s, 1556vs, 1480m, 1409vs, 1367m, 1223m, 1080m, 900m, 780w, 697m, 663mb, 600m, 564w, 442m.

2.3. Single-crystal X-ray crystallography

Data for a selected crystal of **1** were collected at Station 11.3.1 of the Advanced Light Source at Lawrence Berkeley National Laboratory, using a Bruker Apex II CCD diffractometer (ω_O rotation with narrow frames, synchrotron radiation at 0.7749 Å, silicon 111 monochromator). The structure was solved by direct methods and refined using the SHELX-TL suite of programs [21]. All fully occupied non-H atoms were refined anisotropically. All disordered or partially groups were left isotropic to conserve the data to parameter ratio, as the crystal only diffracted to 0.91 Å. In this case the refinement would require extensive restraints to produce nice looking displacement parameters and therefore it seemed more sensible just to leave them isotropic. Hydrogen atoms were placed geometrically on the carbon atoms, then constrained and refined using a riding model. The hydroxyl and water hydrogen atoms could not be found in the difference map nor placed and were therefore omitted from the refinement but not from the chemical formula. O14 is fully occupied, however 60% of the time it is part of a methoxide and 40% is a part of a hydroxide interaction with a partial water (O1W). The programs used for molecular graphics were MERCURY [22] and DIAMOND [23]. Unit cell parameters and structure solution and refinement data for complex **1** are listed in Table 1.

3. Results and discussion

3.1. Synthetic comments

The $Mn/RCO_2^-/teaH_3$ (R = various) reaction system has been extensively studied by many research groups over the last 10 years, under a variety of different conditions, leading to a plethora of high-nuclearity Mn species with impressive structural motifs, appreciable ground-state spin values, and SMM behaviors [24]. On the other hand, the replacement of RCO_2^- groups by N_3^- in the $Mn/teaH_3$ system has only led to two isostructural $Mn^{II/III}_{18}$ clusters reported by Murray [20c] and us [20a]. Recently, we started a program focusing on how the co-presence of azide and carboxylate groups might affect the identity of the products resulted from the $Mn/teaH_3$ general reaction system. Our first results from the investigation of the $Mn/MeCO_2^-/N_3^-/teaH_3$ and $Mn/Bu^tCO_2^-/N_3^-/teaH_3$ reactions have been very encouraging, yielding the compounds $[Mn_{31}O_{19}(OH)(OMe)_6(N_3)_4(O_2CMe)_{23}(tea)_2(dea)_2(MeOH)_2]_n$ ($Mn^{II}_{11}Mn^{III}_{20}$; dea^{2-} is the dianion of

Table 1
Crystallographic data for complex **1**.

Parameter	**1**
Empirical formula	$C_{81.60}H_{157}Mn_{15}Na_2N_{10}O_{48.40}$
M (g mol^{-1})	2922.84
Crystal system	orthorhombic
Space group	$P2_12_12_1$
Unit cell dimensions	
α (Å)	16.8501(19)
b (Å)	25.427(3)
c (Å)	29.736(3)
α (°)	90
β (°)	90
γ (°)	90
V (Å^3)	12740(2)
Z	4
ρ_{calc} (g cm^{-3})	1.524
Radiation, λ (Å)	0.7749[a]
Temperature (K)	150(2)
$2\theta_{max}$ (°)	50.44
μ (mm^{-1})	1.914
F(000)	6003
Total reflections	71633
Unique reflections (R_{int})	17717 (0.0567)
Data with $I > 2\sigma(I)$	14798
Parameters refined	1370
$(\Delta\rho)_{max}/(\Delta\rho)_{min}$ (e Å^{-3})	0.875/−0.520
Goodness-of-fit (GOF) (on F^2)	1.027
R_1,[b] wR_2[c] ($I > 2\sigma(I)$)	0.0527, 0.1368

[a] Synchrotron, 'ALS beamline 11.3.1', 'silicon 111' monochromator.
[b] $R_1 = \sum (||F_o| - |F_c||)/\sum|F_o|$.
[c] $wR_2 = [\sum[w(F_o^2 - F_c^2)^2]/\sum[w(F_o^2)^2]]^{1/2}$, $w = 1/[\sum^2(F_o^2) + [(ap)^2 + bp]$, where $p = [\max(F_o^2, 0) + 2F_c^2]/3$.

diethanolamine) [20a] and $[Mn_{17}NaO_{10}(OH)_2(N_3)_3(O_2CBu^t)_{13}(tea)_3(teaH)(DMF)]$ ($Mn^{II}_4Mn^{III}_{12}Mn^{IV}$), respectively [20a,b].

It is of direct relevance to the present work to discuss the synthetic conditions employed for the isolation of the $\{Mn_{17}Na\}$ cluster mentioned above. Thus, the $\{Mn^{II/III/IV}_{17}Na\}$ compound has been isolated as dark brown plate-like crystals from the reaction of $Mn(ClO_4)_2{\cdot}6H_2O$, $NaO_2CBu^t{\cdot}H_2O$, $teaH_3$, NEt_3 and NaN_3 in a 1:2:1:1:2 molar ratio in MeCN/DMF. The presence of Mn ions in three different oxidation states within the $\{Mn^{II/III/IV}_{17}Na\}$ cage-like cluster, and particularly the stabilization of the rare Mn^{4+} oxidation state, prompted us to perform similar reactions but replacing DMF solvent with the MeOH one. It is well-known that MeOH can reduce high-oxidation state Mn clusters [25], potentially promoting different degrees of cluster aggregation/polymerization [26] and occasionally leading to the solid-state stabilization of oxidation products such as formate ions [27]. Indeed, the reaction of $Mn(ClO_4)_2{\cdot}6H_2O$, $NaO_2CBu^t{\cdot}H_2O$, $teaH_3$, NEt_3 and NaN_3 (1:2:1:1:2) in MeCN/MeOH afforded well-formed brown needle-like crystals of the new complex $[Mn_{15}Na_2O_8(OH)_2(OMe)(N_3)_2(O_2CH)(O_2CBu^t)_{11}(tea)_4(MeOH)]$ (**1**; $Mn^{II}_2Mn^{III}_{13}$, *vide infra*) in good yields (40–45%). The new pentadecanuclear complex **1** is again mixed-valence but contains only Mn^{2+} and Mn^{3+} ions, and includes two Na^+ atoms and a coordinating HCO_2^- group (*vide infra*); the latter most likely results from the metal-assisted oxidation of MeOH [28]. The formation of **1** is summarized in Eq. (1).

$$15Mn^{2+} + 2Na^+ + 4teaH_3 + 19NEt_3 + 2N_3^- + 11Bu^tCO_2^- + 4.25O_2 + 3MeOH + 2.5H_2O \rightarrow [Mn_{15}Na_2O_8(OH)_2(OMe)(N_3)_2(O_2CH)(O_2CBu^t)_{11}(tea)_4(MeOH)] + 19NHEt_3^+ \quad (1)$$

The synthesis involves Mn oxidation, undoubtedly by O_2 under the prevailing basic conditions, and Eq. (1) has been balanced accordingly. The NEt_3 is essential to ensure basic conditions and to act as a proton acceptor to facilitate the deprotonation of the $teaH_3$ groups. A similar role could also be performed by the $Bu^tCO_2^-$ ions, but in the absence of NEt_3 longer reaction times (>24 h) are required to get a significant dark brown coloration, and the yields of isolated **1** are much lower (<10%). On the other hand, more than one equivalent of NEt_3 gave oily products suggestive of mixtures that we have not been able to characterize, or insoluble amorphous precipitates that were probably Mn oxides or oxo/hydroxides. An increase in the amount of $teaH_3$ led to yellow or pale-orange solutions indicative of Mn^{II} products, likely containing mainly or exclusively the neutral $teaH_3$ form of the ligand. Finally, the mixed MeCN/MeOH reaction solvent was identified as the one giving the highest product yield and purity, as well as the best quality single crystals.

3.2. Description of structure

A partially labeled representation of complex **1** is shown in Fig. 1. Selected interatomic distances and angles are listed in Table 2.

Complex **1** crystallizes in the orthorhombic space group $P2_12_12_1$ with the $[Mn_{15}Na_2O_8(OH)_2(OMe)(N_3)_2(O_2CH)(O_2CBu^t)_{11}(tea)_4(MeOH)]$ molecule in a general position. The cage-like structure of **1** comprises a $[Mn_{15}Na_2(\mu_4\text{-}O)_6(\mu_3\text{-}O)_2(\mu_3\text{-}OH)_2(\mu\text{-}OMe)]^{26+}$ core (Fig. 2, top), which can be conveniently dissected into four subunits of three types with an **ABCA** arrangement (Fig. 2, bottom).

The two similar subunits **A** occupy the top and bottom sites of the cage, with each of them comprising two Mn^{III} and a Na^I atoms (Mn7/Mn15/Na2 and Mn8/Mn12/Na1) in a triangular conformation with a capping μ_3-OH^- ion (O10 and O9). The right-side subunit **B** consists of a $[Mn^{II}Mn^{III}_3(\mu_3\text{-}O)_3(\mu\text{-}OMe)]^{4+}$ cubane (Mn9, Mn10, Mn11, Mn14, O6, O7, O8, O14) with an external Mn^{III} atom (Mn13) attached at oxide O8 making the latter quadruply bridging (μ_4) and yielding a $[Mn_5O_3(OMe)]$ subcore. Finally, the left-side subunit **C** comprises a $[Mn^{II}Mn^{III}_3(\mu_3\text{-}O)_3]^{5+}$ defective cubane (cubane missing a vertex; Mn1, Mn4, Mn5, Mn6, O1, O2, O3) which is extended to two opposite sides by binding to two Mn^{III} atoms (Mn2, Mn3) through the 'conversion' of μ_3 O1 and O2 to μ_4; the overall subcore of **C** is thus $[Mn_5O_3]$. Two oxido groups, namely the μ_3-O4 and μ_4-O5, bring the four subunits together, while additional linkage within the **ABCA** arrangement is provided by the alkoxido arms of the four tea^{3-} groups. The latter are of two types: $\eta^2{:}\eta^1{:}\eta^2{:}\eta^2{:}\mu_4$ and $\eta^2{:}\eta^1{:}\eta^2{:}\eta^3{:}\mu_5$ (Fig. 3, top), emphasizing the bridging flexibility of the tea^{3-} group and its ability to bridge

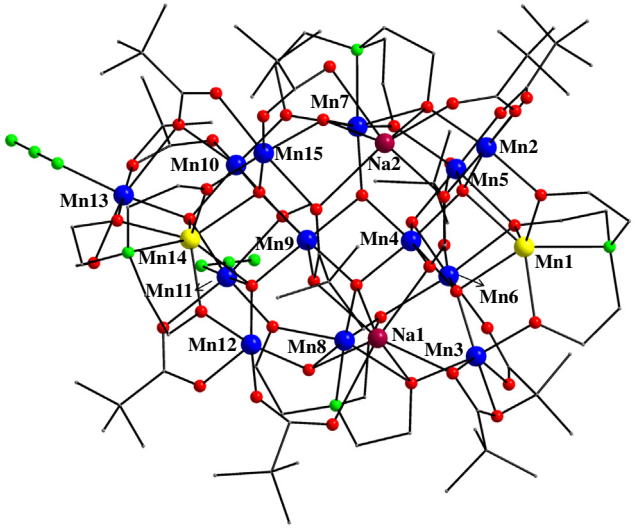

Fig. 1. Partially labeled PovRay representation of complex **1**. H atoms have been omitted for clarity. Color scheme: Mn^{II} yellow; Mn^{III} blue; Na magenta; O red; N green; C grey. (Color online.)

Table 2
Selected interatomic distances (Å) and angles (°) for complex **1**.

Bond lengths			
Mn(1)–O(1)	2.252(8)	Mn(9)–O(14)	2.274(8)
Mn(1)–O(2)	2.268(8)	Mn(9)–O(141)	2.293(8)
Mn(1)–O(11)	2.091(11)	Mn(10)–O(6)	2.112(7)
Mn(1)–O(12)	2.107(10)	Mn(10)–O(8)	1.920(7)
Mn(1)–O(13)	2.169(10)	Mn(10)–O(14)	1.992(8)
Mn(1)–N(11)	2.31(3)	Mn(10)–O(23)	1.902(7)
Mn(2)–O(1)	1.909(8)	Mn(10)–O(162)	2.042(8)
Mn(2)–O(11)	1.943(11)	Mn(10)–O(171)	2.119(8)
Mn(2)–O(21)	1.933(9)	Mn(11)–O(7)	1.943(7)
Mn(2)–O(81)	1.934(10)	Mn(11)–O(8)	1.987(7)
Mn(2)–O(91)	2.152(11)	Mn(11)–O(14)	2.211(8)
Mn(2)–O(202)	2.35(2)	Mn(11)–O(33)	1.921(7)
Mn(3)–O(2)	1.919(8)	Mn(11)–O(181)	2.237(8)
Mn(3)–O(12)	1.901(10)	Mn(11)–N(61)	1.973(10)
Mn(3)–O(31)	1.917(8)	Mn(12)–O(7)	1.877(7)
Mn(3)–O(102)	2.126(9)	Mn(12)–O(9)	1.936(7)
Mn(3)–O(111)	1.971(9)	Mn(12)–O(41)	1.906(8)
Mn(3)–O(112)	2.511(10)	Mn(12)–O(132)	1.941(8)
Mn(4)–O(1)	1.936(8)	Mn(12)–O(182)	2.114(8)
Mn(4)–O(2)	1.970(7)	Mn(13)–O(8)	1.892(7)
Mn(4)–O(3)	2.060(9)	Mn(13)–O(42)	1.876(8)
Mn(4)–O(4)	1.889(7)	Mn(13)–O(162)	2.58(3)
Mn(4)–O(5)	1.891(7)	Mn(13)–O(172)	1.921(8)
Mn(4)–O(201)	2.113(11)	Mn(13)–O(191)	2.163(8)
Mn(5)–O(1)	1.988(8)	Mn(13)–N(71)	1.975(10)
Mn(5)–O(3)	1.868(8)	Mn(14)–O(6)	2.297(7)
Mn(5)–O(13)	2.212(9)	Mn(14)–O(7)	2.428(7)
Mn(5)–O(22)	2.097(8)	Mn(14)–O(8)	2.403(7)
Mn(5)–O(92)	1.930(10)	Mn(14)–O(41)	2.120(8)
Mn(5)–O(121)	1.979(9)	Mn(14)–O(42)	2.156(8)
Mn(6)–O(2)	1.951(8)	Mn(14)–O(43)	2.123(7)
Mn(6)–O(3)	1.860(8)	Mn(14)–N(41)	2.452(9)
Mn(6)–O(13)	2.281(9)	Mn(15)–O(6)	1.864(7)
Mn(6)–O(32)	2.135(8)	Mn(15)–O(10)	1.938(7)
Mn(6)–O(101)	1.941(9)	Mn(15)–O(43)	1.886(8)
Mn(6)–O(122)	1.977(9)	Mn(15)–O(142)	2.325(9)
Mn(7)–O(4)	1.884(7)	Mn(15)–O(151)	1.922(7)
Mn(7)–O(10)	1.924(7)	Mn(15)–O(161)	2.224(8)
Mn(7)–O(21)	2.243(8)	Na(1)–O(5)	2.508(9)
Mn(7)–O(22)	1.910(8)	Na(1)–O(9)	2.571(9)
Mn(7)–O(23)	2.213(7)	Na(1)–O(31)	2.84(3)
Mn(7)–N(21)	2.087(9)	Na(1)–O(112)	2.25(3)
Mn(8)–O(5)	1.883(7)	Na(1)–O(131)	2.669(9)
Mn(8)–O(9)	1.958(8)	Na(1)–O(141)	2.397(3)
Mn(8)–O(31)	2.231(8)	Na(1)–O(201)	2.381(3)
Mn(8)–O(32)	1.901(8)	Na(2)–O(10)	2.296(3)
Mn(8)–O(33)	2.195(8)	Na(2)–O(15B)	2.631(3)
Mn(8)–N(31)	2.068(9)	Na(2)–O(21)	2.527(3)
Mn(9)–O(4)	1.912(7)	Na(2)–O(82)	2.297(3)
Mn(9)–O(5)	1.901(7)	Na(2)–O(142)	2.577(3)
Mn(9)–O(6)	1.898(7)	Na(2)–O(202)	2.21(3)
Mn(9)–O(7)	1.945(7)		
Bond angles			
Mn(1)–O(1)–Mn(2)	101.7(3)	Mn(8)–O(9)–Mn(12)	128.6(4)
Mn(1)–O(1)–Mn(4)	93.1(3)	Mn(9)–O(5)–Na(1)	92.5(3)
Mn(1)–O(1)–Mn(5)	102.1(3)	Mn(9)–O(6)–Mn(10)	100.9(3)
Mn(1)–O(2)–Mn(3)	100.1(3)	Mn(9)–O(6)–Mn(14)	103.0(3)
Mn(1)–O(2)–Mn(4)	91.7(3)	Mn(9)–O(6)–Mn(15)	124.5(4)
Mn(1)–O(2)–Mn(6)	103.9(3)	Mn(9)–O(7)–Mn(11)	108.1(3)
Mn(2)–O(1)–Mn(4)	131.8(4)	Mn(9)–O(7)–Mn(12)	117.8(4)
Mn(2)–O(1)–Mn(5)	122.0(4)	Mn(9)–O(7)–Mn(14)	97.1(3)
Mn(3)–O(2)–Mn(4)	133.4(4)	Mn(9)–O(14)–Mn(10)	92.8(2)
Mn(3)–O(2)–Mn(6)	120.8(4)	Mn(9)–O(14)–Mn(11)	89.1(3)
Mn(4)–O(1)–Mn(5)	98.5(3)	Mn(10)–O(6)–Mn(14)	97.7(3)
Mn(4)–O(2)–Mn(6)	99.1(4)	Mn(10)–O(6)–Mn(15)	124.0(4)
Mn(4)–O(3)–Mn(5)	98.3(4)	Mn(10)–O(8)–Mn(11)	105.3(3)
Mn(4)–O(3)–Mn(6)	99.0(4)	Mn(10)–O(8)–Mn(13)	110.6(3)
Mn(4)–O(4)–Mn(7)	129.8(4)	Mn(10)–O(8)–Mn(14)	99.8(3)
Mn(4)–O(4)–Mn(9)	96.8(3)	Mn(10)–O(14)–Mn(11)	95.1(2)
Mn(4)–O(5)–Na(1)	97.9(3)	Mn(11)–O(7)–Mn(12)	126.8(4)
Mn(4)–O(5)–Mn(8)	131.6(4)	Mn(11)–O(7)–Mn(14)	100.5(3)
Mn(4)–O(5)–Mn(9)	97.1(3)	Mn(11)–O(8)–Mn(13)	135.2(4)
Mn(5)–O(3)–Mn(6)	106.3(4)	Mn(11)–O(8)–Mn(14)	100.0(3)
Mn(7)–O(4)–Mn(9)	124.5(4)	Mn(12)–O(7)–Mn(14)	99.0(3)
Mn(7)–O(10)–Na(2)	100.9(3)	Mn(12)–O(9)–Na(1)	99.3(3)
Mn(7)–O(10)–Mn(15)	129.0(4)	Mn(13)–O(8)–Mn(14)	99.4(3)
Mn(8)–O(5)–Mn(9)	125.2(4)	Mn(14)–O(6)–Mn(15)	101.4(3)
Mn(8)–O(5)–Na(1)	92.6(3)	Mn(15)–O(10)–Na(2)	105.2(3)
Mn(8)–O(9)–Na(1)	88.9(3)		

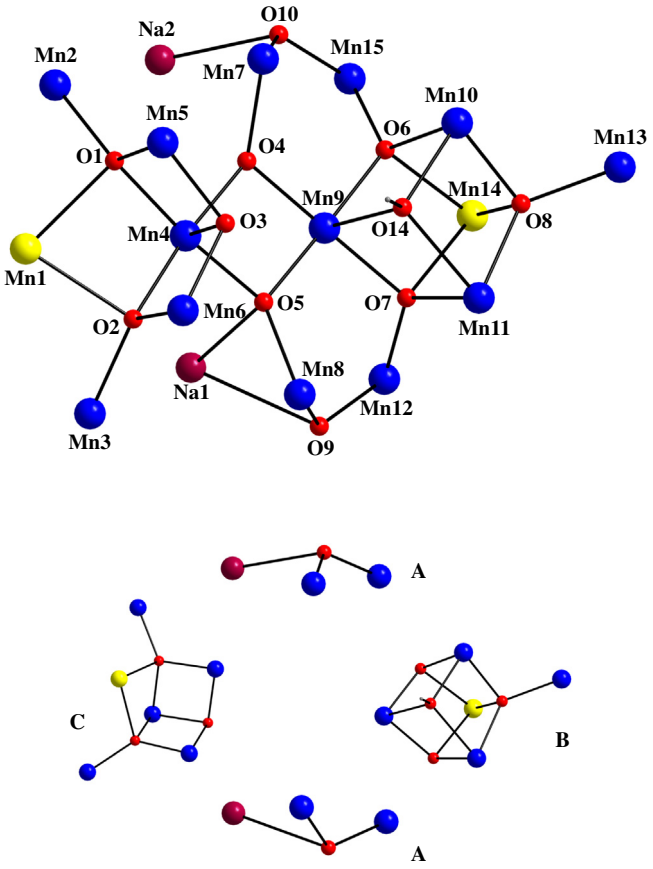

Fig. 2. Partially labeled PovRay representations of (top) the $[Mn_{15}Na_2(\mu_4\text{-}O)_6(\mu_3\text{-}O)_2(\mu_3\text{-}OH)_2(\mu\text{-}OMe)]^{26+}$ core of **1** and (bottom) the three types of constituent subunits of its core. Color scheme: same as in Fig. 1. (Color online.)

multiple metal ions at different oxidation states (i.e. Na^+, Mn^{2+} and Mn^{3+}). Peripheral ligation about the central inorganic core (Fig. 2, top) is provided by eight $\eta^1{:}\eta^1{:}\mu$, an $\eta^1{:}\eta^2{:}\mu$, an $\eta^1{:}\eta^2{:}\mu_3$, and two $\eta^2{:}\eta^2{:}\mu_4$ $Bu^tCO_2^-/HCO_2^-$ groups (Fig. 3, bottom), as well as two terminal N_3^- ions (at Mn11 and Mn13) and a terminal MeOH molecule (at Mn13).

Charge considerations and an inspection of the metric parameters indicate a $2Mn^{II}$, $13Mn^{III}$ description for **1**. This was confirmed quantitatively by bond valence sum (BVS) [29] calculations (Table 3), which identified Mn1 and Mn14 as the Mn^{II} ions, and the others as Mn^{III}. The latter was also consistent with the Jahn–Teller (JT) distortion observed in Mn^{III} ions (Fig. 4), as expected for high-spin d^4 ions in near-octahedral geometry, taking the form of axial elongation of the two *trans* $Mn–O_{alkoxide}$ (either from the alkoxide arms of tea^{3-} groups or from the terminal MeOH molecule) and $Mn–O_{carboxylate}$ bonds (either from pivalate or formate groups). Thus, as is almost always the case, the JT elongation axes avoid the $Mn^{III}–O^{2-}$ bonds, the shortest and strongest in the molecule [30]. In contrast, one of the Mn^{III} atoms, namely the Mn12, is five-coordinate and possesses a square pyramidal geometry ($\tau = 0.05$ [31]). The Mn^{II} atom, Mn1, and Na2 are six-coordinate with distorted octahedral geometries, while the Mn^{II} atom,

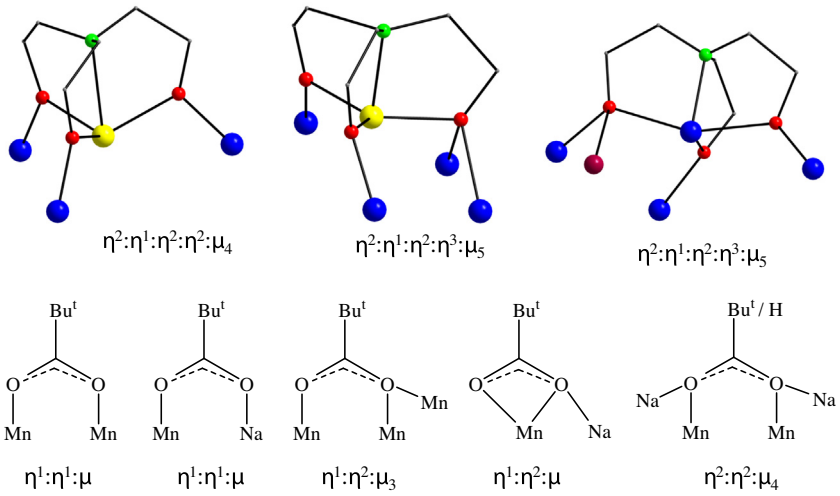

Fig. 3. The coordination modes of tea^{3-} (top) and carboxylate ($Bu^tCO_2^-$ and HCO_2^-) groups found in complex **1**. Color scheme: same as in Fig. 1. (Color online.)

Table 3
Bond valence sum (BVS)[a,b] calculations for Mn, Na, and selected O atoms in **1**.

Atom	Mn^{II}	Mn^{III}	Mn^{IV}
Mn1	2.14	1.98	2.04
Mn2	3.05	2.79	2.92
Mn3	3.07	2.81	2.95
Mn4	3.28	3.08	3.14
Mn5	3.35	3.11	3.19
Mn6	3.19	2.92	3.06
Mn7	3.13	2.90	2.99
Mn8	3.17	2.93	3.03
Mn9	3.26	3.00	3.12
Mn10	3.32	3.07	3.17
Mn11	3.17	2.96	3.02
Mn12	3.10	2.84	2.98
Mn13	3.26	3.02	3.11
Mn14	1.90	1.75	1.82
Mn15	3.29	3.00	3.15
	Mn^{II}	Na^{I}	
Na1	0.98	1.09	
Na2	0.96	1.05	
	BVS	Assignment	
O1	1.86	O^{2-} (μ_4)	
O2	1.83	O^{2-} (μ_4)	
O3	1.73	O^{2-} (μ_3)	
O4	1.83	O^{2-} (μ_3)	
O5	2.00	O^{2-} (μ_4)	
O6	1.85	O^{2-} (μ_4)	
O7	1.87	O^{2-} (μ_4)	
O8	1.83	O^{2-} (μ_4)	
O9	1.19	OH^- (μ_3)	
O10	1.20	OH^- (μ_3)	
O14	1.81	OMe^- (μ_3)	
O191	1.22	MeOH (η^1)	

[a] The underlined value is the one closest to the charge for which it was calculated. The oxidation state is the nearest whole number to the underlined value.
[b] An O BVS in the ~1.7–2.0, ~1.0–1.2, and ~0.2–0.4 ranges is indicative of non-, single- and double-protonation, respectively.

Mn14, and Na1 are seven-coordinate [32] with distorted pentagonal bipyramidal geometries. The protonation level of O^{2-}, OH^-, OMe^-, and MeOH groups was also confirmed by BVS calculations (Table 3). Complex **1** does not form any significant intermolecular interactions of any kind, only a strong intramolecular H-bond between a bridging $Bu^tCO_2^-$ and the terminal MeOH molecule.

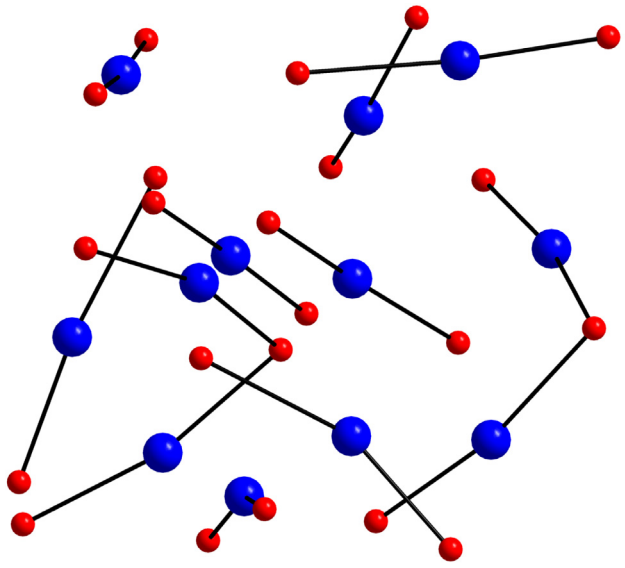

Fig. 4. The orientations of the Jahn–Teller axial elongations for the twelve, six-coordinate Mn^{III} atoms appeared in complex **1**. The view is along the crystallographic *b*-axis. Color scheme: Mn^{III} blue; O red. (Color online.)

Further, the space-filling representation of compound **1** reveals its large nanometer-sized structure and its almost spherical motif with an average diameter of ~1.8 nm as defined by the longest H···H distance.

Complex **1** joins only a handful of previous manganese clusters with a nuclearity of 15. Since most of these were reported only relatively recently, we have listed them in Table 4 for a convenient comparison of their formulae, oxidation states description, and pertinent magnetic data such as their ground state spin (*S*) values and the nature of predominant magnetic exchange interactions. The combined examination of Table 4 and the previously reported in literature results show that **1** possesses an unprecedented metal core topology, is unique in its given oxidation states' level, and exhibits the second largest *S* value among all the other Mn_{15} clusters (*vide infra*). Note that the $Mn^{II}_4Mn^{III}_{11}$ cluster by Tong and coworkers [39] is entirely ferromagnetic with a maximum *S* value of 32, but it does not exhibit an SMM behavior due to the particular arrangement of the Mn^{III} JT axes.

Table 4
Chemical formulae, oxidation states description, ground-state S values, and nature of magnetic exchange interactions for polynuclear Mn complexes with a nuclearity of 15.

Complex[a,b]	Oxidation states	S	Magnetic interactions	Ref.
$[Mn_{15}O_{0.5}(OH)_{11.5}(pao)_{18}(EtOH)(H_2O)]^{6+}$	$Mn^{II}_8Mn^{III}_7$	6	AF (SMM)	[33]
$[Mn_{15}O_6(MePO_3)_2(O_2CMe)_{18}(H_2O)_{12}]^{2+}$	$Mn^{II}_9Mn^{III}_6$	0.5	AF (non-SMM)	[34]
$[Mn_{15}L_{15}(S)_{15}]$	Mn^{III}_{15}	n.r.	n.r.	[35]
$[Mn_{15}O_{17}(OMe)_5(O_2CPh)_{12}(MeOH)_4(H_2O)_5]$	$Mn^{III}_9Mn^{IV}_6$	2	AF (non-SMM)	[36]
$[Mn_{15}O_{17}(OMe)_5(O_2CCh)_{12}(MeOH)_3(H_2O)_6]$	$Mn^{III}_9Mn^{IV}_6$	2	AF (SMM)	[36]
$[Mn_{15}KO_4(O_2CEt)_{11}(pd)_{12}(py)_2]$	$Mn^{II}_4Mn^{III}_{10}Mn^{IV}$	11.5	F (SMM)	[37]
$[Mn_{15}O_8(OMe)_6(Bu^tPO_3)_{10}(dmbpy)_2]$	$Mn^{II}_3Mn^{III}_{12}$	n.r.	AF (SMM)	[38]
$[Mn_{15}Na_2O_8(HL')_{10}(O_2CMe)_2(H_2O)_2(OMe)_{1.5}(N_3)_{2.5}]^+$	$Mn^{II}_4Mn^{III}_{11}$	32	F (non-SMM)	[39]
$[Mn_{15}Na_2O_8(OH)_2(OMe)(N_3)_2(O_2CH)(O_2CBu^t)_{11}(tea)_4(MeOH)]$	$Mn^{II}_2Mn^{III}_{13}$	14	F (SMM)	t.w.

[a] Counterions and solvate molecules are omitted.
[b] *Abbreviations:* F = ferromagnetic; AF = antiferromagnetic; n.r. = not reported; t.w. = this work; paoH = 2-pyridinealdoxime; LH_3 = N-phenylpropiolyl salicylhydrazide; S = DMF or H_2O; $ChCO_2H$ = cyclohexanecarboxylic acid; pdH_2 = 1,3-propanediol; py = pyridine; dmbpy = 4,4′-dimethyl-2,2′-bipyridyl; H_3L' = 2,6-(hydroxymethyl)phenol.

3.3. Magnetochemistry

3.3.1. Dc magnetic susceptibility studies

Solid-state, variable-temperature magnetic susceptibility measurements were performed on a vacuum-dried microcrystalline sample of **1**, which was suspended in eicosane to prevent torquing. The dc (direct current) magnetic susceptibility (χ_M) data were collected in the temperature range of 5.0–300 K, in a 0.1 T magnetic field and are plotted as $\chi_M T$ versus T in Fig. 5. The $\chi_M T$ value at 300 K is 48.24 $cm^3\,K\,mol^{-1}$ and is very close to the spin-only ($g = 2$) value of 47.75 $cm^3\,K\,mol^{-1}$ expected for a Mn_{15} unit comprising two Mn^{II} and thirteen Mn^{III} non-interacting ions. The $\chi_M T$ value then increases gradually with decreasing temperature to a maximum of 97.84 $cm^3\,K\,mol^{-1}$ at 8 K, before decreasing to 95.98 $cm^3\,K\,mol^{-1}$ at 5.0 K. This behavior is indicative of the presence of dominant ferromagnetic exchange interactions in **1**. In addition, the maximum of 97.84 $cm^3\,K\,mol^{-1}$ at 8 K suggests that **1** possesses a large spin ground state value of $S = 13$ or 14; the spin-only ($g = 2$) values for $S = 13$ and 14 are 91 and 105 $cm^3\,K\,mol^{-1}$, respectively. The small decrease of $\chi_M T$ at low temperatures (<8 K) is likely due to zero-field splitting (ZFS), Zeeman effects from the applied field, and/or any weak intermolecular interactions. Given the size and the low-symmetry of the Mn_{15} molecule, and the resulting number of inequivalent exchange constants, it is not possible to apply the Kambe method to determine the individual pairwise exchange interaction parameters between the Mn ions; direct matrix diagonalization methods are also computationally unfeasible.

To determine the ground state of **1**, magnetization (M) versus dc field measurements were made on restrained samples in the magnetic field (H) and temperature ranges of 1.8–10.0 K and 1.0–70.0 kG (0.1–7 T). The resulting data are shown in Fig. 6 as a reduced magnetization ($M/N\mu_B$) versus H/T plot, where N is Avogadro's number and μ_B is the Bohr magneton. The data were fit using the program MAGNET [40], which assumes that only the ground state is populated at these temperatures, includes axial zero-field splitting ($D\hat{S}_z^2$) and isotropic Zeeman interactions with the applied field, and carries out a full powder average. The corresponding Hamiltonian is given by Eq. (2)

$$\mathscr{H} = D\hat{S}_z^2 + g\mu_B\mu_0\hat{S}\cdot H \tag{2}$$

where D is the axial ZFS parameter, $\hat{S}_z$ is the easy-axis spin operator, g is the electronic g factor, μ_0 is the vacuum permeability, and H is the applied field. The last term in Eq. (2) is the Zeeman energy associated with an applied magnetic field. However, we could not get an acceptable fit using data collected over the whole field range, which is a common problem caused by the existence of low-lying excited states or/and intermolecular interactions. As has been described elsewhere on multiple occasions for mixed-valence $Mn^{II/III}$ clusters [6b,7b,11b,19,20,24–28,37] a common solution to this problem is to use only data collected at low fields. Indeed, a reasonable fit of the reduced magnetization data could be achieved when data collected in fields only up to 2.0 T were employed. The fit is shown as the solid line in Fig. 6 and the fit parameters were $S = 14$, $D = -0.063(1)\,cm^{-1}$ and $g = 1.97(1)$, slightly less than 2.0 as expected for mixed-valence $Mn^{II/III}$ complexes [16]. Attempts were also made to fit the data assuming an $S = 13$ or 15 spin ground state; however, the resulting fits were of much poorer quality and gave

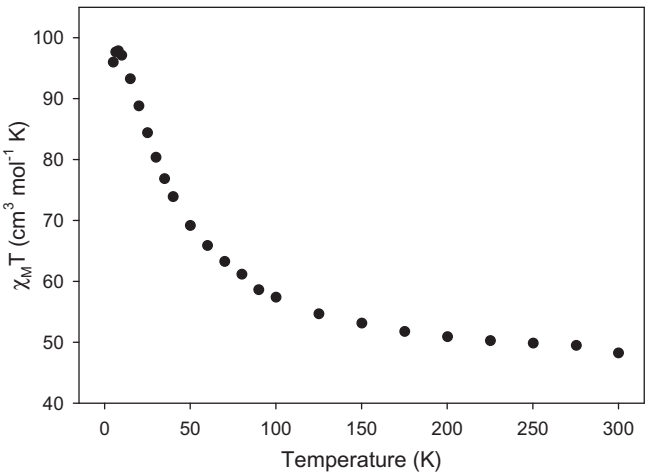

Fig. 5. Plot of $\chi_M T$ vs. T for **1** in a 1 kG field.

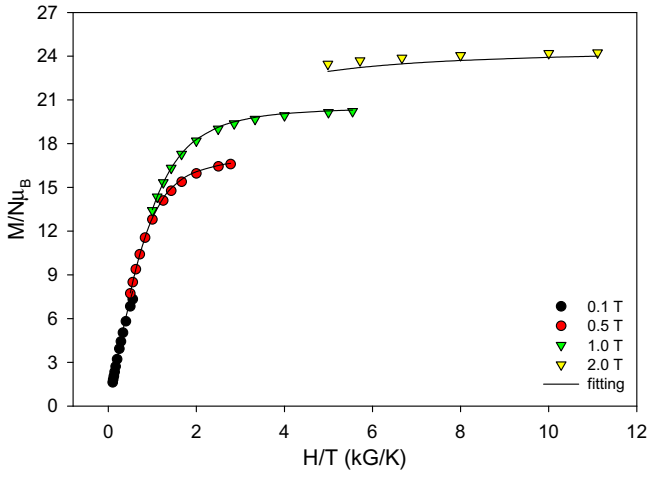

Fig. 6. Plot of reduced magnetization ($M/N\mu_B$) vs. H/T for complex **1** at applied fields of 0.1–2.0 T and in the 1.8–10.0 K temperature range. The solid lines are the fit of the data; see the text for the fit parameters.

too small (<1.82) or too large (>2.06) for Mn clusters g values, respectively.

As has been described in several previous cases [6b,7b, 11b,19,20,24–28,37], ac (alternating current) susceptibility studies provide a powerful complement to dc studies for determining the ground state of a system because they preclude any complications arising from the presence of a dc field. Therefore, we carried out detailed ac studies on complex **1** in order to determine independently its ground state S and also to detect the slow magnetization relaxation suggestive of SMM behavior.

3.3.2. Ac magnetic susceptibility studies

Alternating current studies were performed in the 1.8–15 K range using a 3.5 G ac field oscillating at frequencies in the 50–1000 Hz range. If the magnetization vector can relax fast enough to keep up with the oscillating field, then there is no imaginary (out-of-phase) susceptibility signal (χ''_M), and the real (in-phase) susceptibility (χ'_M) is equal to the dc susceptibility [41]. The $\chi'_M T$ extrapolated from a temperature high enough to avoid the effects of any weak intermolecular interactions or slow relaxation to 0 K (where only the ground state would be populated) should thus be in agreement with the formula $\chi'_M T = g^2 S(S+1)/8$, where S is the ground state of the compound. However, if the barrier to magnetization relaxation is significant compared to thermal energy (kT), then there is a non-zero χ''_M signal and the in-phase signal decreases. In addition, the χ''_M signal will be frequency-dependent. Such frequency-dependent χ''_M signals are a characteristic signature of the superparamagnetic-like properties of a SMM (but by themselves do not prove the presence of a SMM [42]).

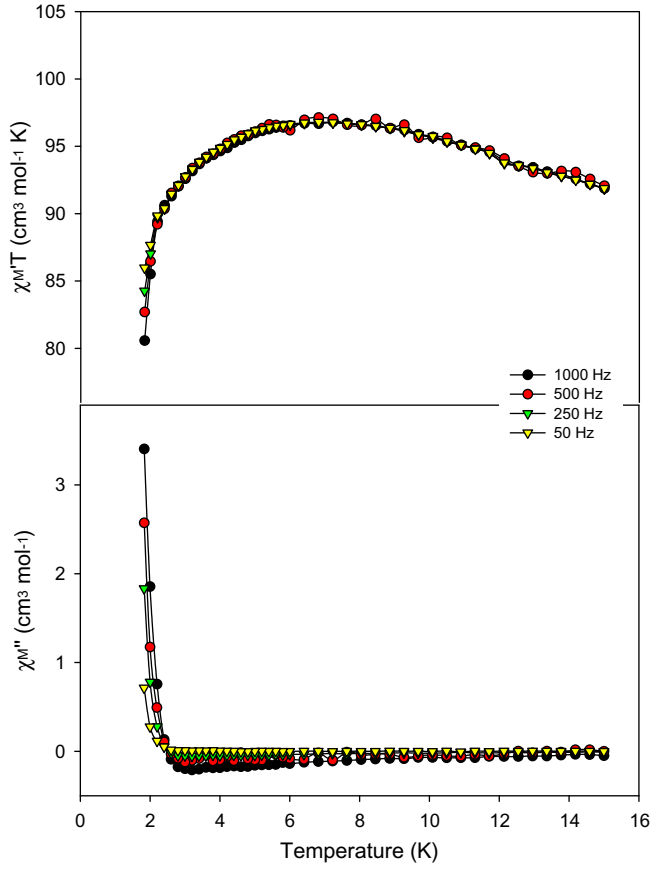

Fig. 7. Plots of the in-phase (χ'_M) as $\chi'_M T$ (top) and out-of-phase (χ''_M) (bottom) ac magnetic susceptibilities vs. T for complex **1** in a 3.5 G field oscillating at the indicated frequencies.

For complex **1**, the in-phase signal (χ'_M, plotted as $\chi'_M T$ versus T, Fig. 7, top) increases slightly from ~92 cm^3 K mol^{-1} at 15 K to ~97 cm^3 K mol^{-1} at 8 K, followed by a plateau until ~6 K, and then decreases rapidly at temperatures lower than ~5 K. The small increase of the $\chi'_M T$ values is most likely due to depopulation of excited states with spin S smaller than that of the ground state. The rapid decrease of the $\chi'_M T$ below ~5 K is due to ZFS and any weak intermolecular interactions. In addition, below ~2.5 K there is a frequency-dependent decrease in $\chi'_M T$ and a concomitant appearance of frequency-dependent χ''_M signals (Fig. 7, bottom). However, only the beginnings of peaks appear above 1.8 K (the operating minimum temperature of our SQUID magnetometer), with the peak maxima clearly lying at lower temperatures. Such tails of signals are an indication of the superparamagnetic-like slow relaxation of an SMM, but one with a rather small relaxation barrier. Further confirmation of the SMM behavior would require single-crystal studies on a micro-SQUID apparatus [43], but this was not pursued because there are now many SMMs with such small relaxation barriers. Extrapolation to 0 K of $\chi'_M T$ from values above 8 K, to avoid complications from effects such as intermolecular interactions and ZFS at lower temperatures, gives a value of ~104 cm^3 K mol^{-1}, indicative of a ground spin state of $S = 14$ with g ~1.99, in satisfying agreement with the results obtained by the dc magnetization fits.

4. Conclusions and perspectives

The present work extends the body of results that emphasize the ability of $teaH_3$ to form interesting structural types in Mn cluster chemistry. In addition to the recently reported $[Mn_{17}NaO_{10}(OH)_2(N_3)_3(O_2CBu^t)_{13}(tea)_3(teaH)(DMF)]$ [20a,b] cluster, the $Mn/Bu^tCO_2^-/N_3^-/teaH_3$ reaction system has provided further access to the new pentadecanuclear compound **1**, upon changing the reaction solvent mixture from MeCN/DMF to MeCN/MeOH. The reported cluster clearly supports the pronounced ability of tea^{3-} anion to stabilize high-nuclearity Mn species when combined with various ancillary groups such as carboxylates and azides. Complex **1** is novel in multiple ways, as described, but also provides a rare example of a ferromagnetic, high-nuclearity mixed-valence $Mn^{II/III}$ cluster with a large ground-state spin value of $S = 14$. Due to the complexity of the Mn_{15} structure and the multiple fused triangular subunits, textbook examples of a topology that can give spin frustration effects (competing exchange interactions), any attempts to rationalize the observed S value shall fall into inaccuracies. Nevertheless, such magnetostructural complications are often observed in molecular cluster chemistry, but these have not prevented synthetic chemists from making more and more nanometer-sized compounds with aesthetically-pleasing structures and impressive physical properties.

We are currently investigating how the substitution of $Bu^tCO_2^-$ groups by various other such groups, less employed before in Mn cluster chemistry, might affect the identity of isolated $Mn/teaH_3/N_3^-$ products, and to what extent this might prove a route to new cluster types.

Acknowledgements

D.I.A and Th.C.S thank the Ontario Trillium Foundation for a graduate scholarship (to D.I.A). The Advanced Light Source is supported by The Director, Office of Basic Energy Sciences, of the U.S. Department of Energy under Contract No. DE-AC02-05CH11231.

Appendix A. Supplementary data

CCDC 920881 contains the supplementary crystallographic data for **1**. These data can be obtained free of charge via http://

www.ccdc.cam.ac.uk/conts/retrieving.html, or from the Cambridge Crystallographic Data Centre, 12 Union Road, Cambridge CB2 1EZ, UK; fax: (+44) 1223-336-033; or e-mail: deposit@ccdc.cam.ac.uk.

References

[1] (a) R. Sessoli, H.-L. Tsai, A.R. Schake, S. Wang, J.B. Vincent, K. Folting, D. Gatteschi, G. Christou, D.N. Hendrickson, J. Am. Chem. Soc. 115 (1993) 1804;
(b) G. Christou, D. Gatteschi, D.N. Hendrickson, R. Sessoli, MRS Bull. 25 (2000) 66.

[2] For a comprehensive review, see: R. Bagai, G. Christou, Chem. Soc. Rev. 38 (2009) 1011.

[3] (a) W. Wernsdorfer, N. Aliaga-Alcalde, D.N. Hendrickson, G. Christou, Nature 416 (2002) 406;
(b) S. Hill, R.S. Edwards, N. Aliaga-Alcalde, G. Christou, Science 302 (2003) 1015.

[4] (a) M.A. Bolcar, S.M.J. Aubin, K. Folting, D.N. Hendrickson, G. Christou, J. Chem. Soc., Chem. Commun. (1997) 1485;
(b) E.K. Brechin, J. Yoo, M. Nakano, J.C. Huffman, D.N. Hendrickson, G. Christou, Chem. Commun. (1999) 783;
(c) M. Murugesu, M. Habrych, W. Wernsdorfer, K.A. Abboud, G. Christou, J. Am. Chem. Soc. 126 (2004) 4766;
(d) Th.C. Stamatatos, K.A. Abboud, W. Wernsdorfer, G. Christou, Angew. Chem., Int. Ed. 45 (2006) 4134.

[5] A.J. Tasiopoulos, A. Vinslava, W. Wernsdorfer, K.A. Abboud, G. Christou, Angew. Chem., Int. Ed. 43 (2004) 2117.

[6] (a) Th.C. Stamatatos, D. Foguet-Albiol, C.C. Stoumpos, C.P. Raptopoulou, A. Terzis, W. Wernsdorfer, S.P. Perlepes, G. Christou, J. Am. Chem. Soc. 127 (2005) 15380;
(b) Th.C. Stamatatos, K.A. Abboud, W. Wernsdorfer, G. Christou, Angew. Chem., Int. Ed. 46 (2007) 884.

[7] (a) A. Mishra, W. Wernsdorfer, K.A. Abboud, G. Christou, J. Am. Chem. Soc. 126 (2004) 15648;
(b) Th.C. Stamatatos, S.J. Teat, W. Wernsdorfer, G. Christou, Angew. Chem., Int. Ed. 48 (2009) 521.

[8] (a) G. Christou, J.B. Vincent, Metal clusters in proteins, in: L. Que (Ed.), ACS Symp. Ser., vol. 372, American Chemical Society, 1988, pp. 238–255 (Chapter 12);
(b) A. Mishra, W. Wernsdorfer, K.A. Abboud, G. Christou, Chem. Commun. (2005) 54.

[9] S. Mukherjee, J.A. Stull, J. Yano, Th.C. Stamatatos, K. Pringouri, T.A. Stich, K.A. Abboud, R.D. Britt, V.K. Yachandra, G. Christou, Proc. Nat. Acad. Sci. U.S.A. 109 (2012) 2257.

[10] G. Maayan, G. Christou, Inorg. Chem. 20 (2011) 7015.

[11] (a) For representative examples from current independent scientists who have been students or post-doctoral associates of G. Christou, see: E.S. Koumousi, S. Mukherjee, C.M. Beavers, S.J. Teat, G. Christou, Th.C. Stamatatos, Chem. Commun. 47 (2011) 11128;
(b) E.E. Moushi, C. Lampropoulos, W. Wernsdorfer, V. Nastopoulos, G. Christou, A.J. Tasiopoulos, J. Am. Chem. Soc. 132 (2010) 16146;
(c) J. Long, F. Habib, P.-H. Lin, I. Korobkov, G. Enright, L. Ungur, W. Wernsdorfer, L.F. Chibotaru, M. Murugesu, J. Am. Chem. Soc. 133 (2011) 5319;
(d) C.J. Milios, A. Vinslava, W. Wernsdorfer, S. Moggach, S. Parsons, S.P. Perlepes, G. Christou, E.K. Brechin, J. Am. Chem. Soc. 129 (2007) 2754;
(e) J. Sánchez Costa, L.A. Barrios, G.A. Craig, S.J. Teat, F. Luis, O. Roubeau, M. Evangelisti, A. Camón, G. Aromí, Chem. Commun. 48 (2012) 1413;
(f) M. Menelaou, F. Ouharrou, L. Rodríguez, O. Roubeau, S.J. Teat, N. Aliaga-Alcalde, Chem. Eur. J. 18 (2012) 11545;
(g) V. Chandrasekhar, A. Dey, T. Senapati, E.C. Sañudo, Dalton Trans. 41 (2012) 799.

[12] J.R. Friedman, M.P. Sarachik, J. Tejada, R. Ziolo, Phys. Rev. Lett. 76 (1996) 3830.

[13] (a) W. Wernsdorfer, R. Sessoli, Science 284 (1999) 133;
(b) W. Wernsdorfer, M. Soler, G. Christou, D.N. Hendrickson, J. Appl. Phys. 91 (2002) 7164.

[14] G. Christou, Polyhedron 24 (2005) 2065.

[15] (a) L. Bogani, W. Wernsdorfer, Nat. Mater. 7 (2008) 179;
(b) M.N. Leuenberger, D. Loss, Nature 410 (2001) 789.

[16] Th.C. Stamatatos, G. Christou, Philos. Trans. R. Soc. A 366 (2008) 113.

[17] For a mini-review of azide groups in higher oxidation state manganese cluster chemistry see: Th.C. Stamatatos, G. Christou, Inorg. Chem. 48 (2009) 3308. and references cited therein.

[18] (a) A. Escuer, G. Aromi, Eur. J. Inorg. Chem. (2006) 4721;
(b) J. Ribas, A. Escuer, M. Monfort, R. Vicente, R. Cortes, L. Lezama, T. Rojo, Coord. Chem. Rev. 193–195 (1999) 1027;
(c) X.-Y. Wang, Z.-M. Wang, S. Gao, Chem. Commun. (2008) 281;
(d) Y.-F. Zeng, X. Hu, F.-C. Liu, X.-H. Bu, Chem. Soc. Rev. 38 (2009) 469.

[19] (a) For example, see: S. Schmidt, D. Prodius, G. Novitchi, V. Mereacre, G.E. Kostakis, A.K. Powell, Chem. Commun. 48 (2012) 9825;
(b) V. Mereacre, D. Prodius, Y. Lan, C. Turta, C.E. Anson, A.K. Powell, Chem. Eur. J. 17 (2011) 123;
(c) M.I. Khan, S. Tabussum, R.J. Doedens, V.O. Golub, C.J. O'Connor, Inorg. Chem. Commun. 7 (2004) 54;
(d) A. Baniodeh, I.J. Hewitt, V. Mereacre, Y. Lan, G. Novitchi, C.E. Anson, A.K. Powell, Dalton Trans. 40 (2011) 4080;
(e) W.-G. Wang, A.-J. Zhou, W.-X. Zhang, M.-L. Tong, X.-M. Chen, M. Nakano, C.C. Beedle, D.N. Hendrickson, J. Am. Chem. Soc. 129 (2007) 1014;
(f) L.F. Jones, P. Jensen, B. Moubaraki, K.J. Berry, J.F. Boas, J.R. Pilbrow, K.S. Murray, J. Mater. Chem. 16 (2006) 2690;
(g) S.K. Langley, N.F. Chilton, B. Moubaraki, K.S. Murray, Dalton Trans. 41 (2012) 1033.

[20] (a) Th.C. Stamatatos, D. Foguet-Albiol, W. Wernsdorfer, K.A. Abboud, G. Christou, Chem. Commun. 47 (2011) 274;
(b) Th.C. Stamatatos, K.A. Abboud, G. Christou, Polyhedron 28 (2009) 1880;
(c) S.K. Langley, K.J. Berry, B. Moubaraki, K.S. Murray, Dalton Trans. (2009) 973.

[21] Bruker AXS Inc., Madison, WI, 2003.

[22] MERCURY; I.J. Bruno, J.C. Cole, P.R. Edgington, M.K. Kessler, C.F. Macrae, P. McCabe, J. Pearson, R. Taylor, Acta Crystallogr., Sect. B 58 (2002) 389.

[23] K. Bradenburg, DIAMOND, Release 3.1f, Crystal Impact GbR, Bonn, Germany, 2008.

[24] (a) L.M. Wittick, L.F. Jones, P. Jensen, B. Moubaraki, L. Spiccia, K.J. Berry, K.S. Murray, Dalton Trans. (2006) 1534;
(b) C.C. Beedle, K.J. Heroux, M. Nakano, A.G. DiPasquale, A.L. Rheingold, D.N. Hendrickson, Polyhedron 26 (2007) 2200;
(c) L.M. Wittick, K.S. Murray, B. Moubaraki, S.R. Batten, L. Spiccia, K.J. Berry, Dalton Trans. (2004) 1003;
(d) G. Rajaraman, M. Murugesu, E.C. Sañudo, M. Soler, W. Wernsdorfer, M. Helliwell, C. Muryn, J. Raftery, S.J. Teat, G. Christou, E.K. Brechin, J. Am. Chem. Soc. 47 (2004) 15445;
(e) M. Murugesu, W. Wernsdorfer, K.A. Abboud, G. Christou, Angew. Chem., Int. Ed. 44 (2005) 892;
(f) S.J. Shah, C.M. Ramsey, K.J. Heroux, J.R. O'Brien, A.G. DiPasquale, A.L. Rheingold, E. del Barco, D.N. Hendrickson, Inorg. Chem. 47 (2008) 6245;
(g) A.M. Ako, V. Mereacre, I.J. Hewitt, R. Clerac, L. Lecren, C.E. Anson, A.K. Powell, J. Mater. Chem. 16 (2006) 2579;
(h) S.K. Langley, B. Moubaraki, K.J. Berry, K.S. Murray, Dalton Trans. 39 (2010) 4848;
(i) S.K. Langley, N.F. Chilton, M. Massiamiliano, B. Moubaraki, K.J. Berry, K.S. Murray, Dalton Trans. 39 (2010) 7236.

[25] A.J. Tasiopoulos, W. Wernsdorfer, K.A. Abboud, G. Christou, Inorg. Chem. 44 (2005) 6324.

[26] (a) P. King, W. Wernsdorfer, K.A. Abboud, G. Christou, Inorg. Chem. 43 (2004) 7315;
(b) A.J. Tasiopoulos, W. Wernsdorfer, K.A. Abboud, G. Christou, Angew. Chem., Int. Ed. 43 (2004) 6338.

[27] N.E. Chakov, L.N. Zakharov, A.L. Rheingold, K.A. Abboud, G. Christou, Inorg. Chem. 44 (2005) 4555.

[28] (a) For example, see: B. Biswas, S. Khanra, T. Weyhermüller, P. Chaudhuri, Chem. Commun. (2007) 1059;
(b) C. Papatriantafyllopoulou, Th.C. Stamatatos, W. Wernsdorfer, S.J. Teat, A.J. Tasiopoulos, A. Escuer, S.P. Perlepes, Inorg. Chem. 49 (2010) 10486.

[29] (a) W. Liu, H.H. Thorp, Inorg. Chem. 32 (1993) 4102;
(b) I.D. Brown, D. Altermatt, Acta Crystallogr., Sect. B (1985) 244.

[30] (a) N.E. Chakov, S.-C. Lee, A.G. Harter, P.L. Kuhns, A.P. Reyes, S.O. Hill, N.S. Dalal, W. Wernsdorfer, K.A. Abboud, G. Christou, J. Am. Chem. Soc. 128 (2006) 6975;
(b) Th.C. Stamatatos, B.S. Luisi, B. Moulton, G. Christou, Inorg. Chem. 47 (2008) 1134.

[31] A.W. Addison, T.N. Rao, J. Reedijk, J.V. Rijin, G.C. Verschoor, J. Chem. Soc., Dalton Trans. (1984) 1349.

[32] Th.C. Stamatatos, K.A. Abboud, G. Christou, J. Cluster Sci. 21 (2010) 485.

[33] D.I. Alexandropoulos, C. Papatriantafyllopoulou, G. Aromi, O. Roubeau, S.J. Teat, S.P. Perlepes, G. Christou, Th.C. Stamatatos, Inorg. Chem. 49 (2010) 3962.

[34] M. Wang, C. Ma, H. Wen, C. Chen, Dalton Trans. (2009) 994.

[35] R.P. John, M. Park, D. Moon, K. Lee, S. Hong, Y. Zou, C.S. Hong, M.S. Lah, J. Am. Chem. Soc. 129 (2007) 14142.

[36] Y.-Z. Zheng, W. Xue, W.-X. Zhang, M.-L. Tong, X.-M. Chen, Inorg. Chem. 46 (2007) 6437.

[37] E.E. Moushi, A. Masello, W. Wernsdorfer, V. Nastopoulos, G. Christou, A.J. Tasiopoulos, Dalton Trans. 39 (2010) 4978.

[38] F.A. Mautner, R.C. Fischer, M. Salah El Fallah, S. Speed, R. Vicente, Polyhedron 36 (2012) 92.

[39] J.-L. Liu, J.-D. Leng, Z. Lin, M.-L. Tong, Chem. Asian J. 6 (2011) 1007.

[40] E.R. Davidson, MAGNET, Indiana University, Bloomington, IN, 1999.

[41] M.A. Novak, R. Sessoli, in: L. Gunther, B. Barbar (Eds.), Quantum Tunnelling of Magnetization, QTM'94, Kluwer, Dordrecht, The Netherlands, 1995, pp. 171–188.

[42] (a) N.E. Chakov, W. Wernsdorfer, K.A. Abboud, G. Christou, Inorg. Chem. 43 (2004) 5919;
(b) A. Mishra, A.J. Tasiopoulos, W. Wernsdorfer, K.A. Abboud, G. Christou, Inorg. Chem. 46 (2007) 3105.

[43] W. Wernsdorfer, Adv. Chem. Phys. 118 (2001) 99.